Constitutive analysis of biomedical grade Co-27Cr-5Mo alloy at high strain rates

D. Trimble[1], H. Shipley[1], L. Lea[2], A. Jardine[2], G. E O'Donnell[1]

[1]Department of Mechanical & Manufacturing Engineering
Trinity College Dublin, Ireland
[2] Department of Physics, Cavendish Laboratory, University of Cambridge, United Kingdom.

*Corresponding author. Tel: +353 1 8964856
E-mail address: dtrimble@tcd.ie (D. Trimble)

Abstract:

Cobalt Chrome is used extensively within the biomedical industry for hip, knee and shoulder prostheses. These components are manufactured using a range of different processes which includes machining. In order to develop Finite Element Models of machining processes, it is necessary to develop the constitutive model of the workpiece material at high strain rates over different temperatures. During this research, Split Hopkinson Pressure Bar tests were conducted over a wide processing domain of temperatures (298-873 K) and strain-rates (600-1400s^{-1}) to predict the constitutive model of biomedical grade Cobalt Chrome based on modified Zerilli-Armstrong, modified Johnson-Cook and strain compensated Arrhenius-type models. The prediction capability of these models was evaluated in terms of average absolute relative error and correlation coefficient between predicted and experimental flow stress values. Results demonstrated that the modified Zerilli-Armstrong model can track the deformational behaviour more accurately throughout the entire processing domain investigated compared to the other models. The model recorded an average absolute relative error of 2.71% and a correlational coefficient of 0.98.

Keywords: Cobalt Chrome; flow stress; constitutive equation; Co-27Cr-5Mo.

1. Introduction

Due to their excellent mechanical properties, wear resistance and biocompatibility, cobalt chrome (CoCr) alloys are used extensively within the biomedical industry. Applications include bone plates, dental devices , components of hip, knee and shoulder prostheses as well as some cardiovascular prostheses [1–3]. During manufacturing processes, CoCr alloys are subjected to strain rates ranging from 10^{-1} to 10^{6} [4]. Further, these alloys are commonly associated with poor machinability with short tool life and poor surface finish leading to low productivity and high manufacturing costs [5]. Nevertheless, presently there is little quantitative deformational data of CoCr alloys over a large processing range of temperatures and strain rates which are requisite for constitutive equation development.

Constitutive equations are mathematical representations describing the relationship between the flow stress, strain rate and temperature of a material [6]. They describe the thermo mechanical behaviour of materials during machining processes in a form that is incorporated into finite element (FE) software [7,8]. However, the accuracy of such FE models is a constant concern. Material models are frequently extrapolated outside their calibration range, leading to poor prediction accuracy at high strain rates which are typical of machining metal alloys [7]. Currently, there are three broad categories of models to construct constitutive relationships for a myriad of metals and alloys; physical, empirical/semi-empirical and phenomenological [9]. The ideal constitutive equation contains a reasonable number of material constants, which are evaluated using a limited number of experimental data to represent the flow behaviour of a material over a broad range of temperature and strain values [10].

Physical based models such as the Mechanical Threshold Stress (MTS) model [11] allow for an accurate definition of material behaviour under a broad range of loading conditions. Yet they are not always preferred as they require physical assumptions and a large number of material constants from precisely controlled experiments [12,13]. Phenomenological models such as the Arrhenius Type (AT) equation are widely adopted in practice as they are less strictly related to physical phenomena but produce satisfactory accuracies in flow predictions. More importantly, they only need to calculate a reasonable number of material constants with limited experimental results [9]. Empirical and semi-empirical models, in particular the Johnson-Cook (JC) model [14] and Zerilli-Armstrong (ZA) model [15] are frequently utilized in commercially available FE software [16]. They provide a definition of flow stress based on empirical observations and require a reduced number of material constants providing for easy calibration [17].

The original JC model assumes that strain rate hardening, thermal softening and strain hardening are independent metallurgical phenomena and are subsequently isolated from each other. However, the coupled effects of; strain rate, temperature and strain on the flow stress of cobalt chromium should be considered in order to provide an accurate prediction of deformation behaviour [18]. To account for these coupled effects many authors have modified the original JC equation for a variety of materials [18–23]. Among them, Song et al. [19] modified the original JC model by coupling the effects of temperature and strain rate. Their model displayed good agreement with experimental results obtained at elevated temperatures and high strain rates using a split Hopkinson pressure bar [18].

The Zerilli-Armstrong (ZA) model [15] is a popular semi-empirical constitutive model which incorporates the coupled effects of strain rate and temperature as well as the dislocation characteristics for particular structures. However, some material constants required for the ZA model are difficult to validate as they require a stress at 0K as well as the athermal stress of the materials [24]. Furthermore the ZA model is incapable of predicting flow stress for temperatures

above half the melting temperature of the material with the absolute error raising to approximately 10% [25]. Consequently, Samantaray et al. [12] proposed a modified ZA (mZA) model which considers the effects of thermal softening, strain rate hardening and isotropic hardening as well as the coupled effects of temperature and strain and of strain rate and temperature on flow stress. In a further study comparing the abilities of the JC, mZA and Arrhenius type equation to represent elevated temperature flow behaviour, Samantaray et al. [16] concluded that the mZA was in good agreement with experimental data and that the computational time required to evaluate the model constants was several times less than that of the Arrhenius type equation. Furthermore, Zhan et al. [24] successfully used the mZA model to predict the flow behaviour of Ti6554 alloy over a wide range of temperature (293-1173K) and strain rates ($10^3 - 10^4 s^{-1}$) typical of those experienced during processing of CoCr alloys.

Jonas et al. [26] proposed a phenomenological approach whereby the flow stress is expressed by the hyperbolic laws in an Arrhenius type equation and it has been applied successfully to predict the flow stress of various materials [16,27]. However, the effects of strain are ignored leading to inaccurate predictions when dynamic softening appears during hot deformation [9,28]. Accordingly, the original model has been revised several times by different authors, including Zener and Hollomon [29], who introduced the parameter Z, to account for the relationship between strain rate and temperature. Similarly, Sloof et al. [30] incorporated a strain dependent parameter enabling accurate predictions of flow stress during deformation for a wide range of temperature and strain values. Lin et al. [31], Shi et al. [32] and Mandal et al. [27] amongst others have successfully employed the strain and strain rate compensated Arrhenius type (ATC) equation to accurately predict flow stress behaviour of an assortment of materials for a broad collection of temperature and strain values.

To date, the constitutive equation of the present biomedical grade Co-27Cr-5Mo alloy does not exist in open literature and is required for the purpose of FE modelling. Therefore, the objective of this investigation was to determine the flow stress of the present alloy through Split Hopkinson Pressure Bar tests over a wide processing range of temperatures and strain rates to establish the constitutive equation based on modified *JC*, modified *ZA* and strain compensated *AT* models. The reliability of these models were also evaluated in terms of average absolute relative error (*AARE*) and correlation coefficient (*R*).

2. Experimental material and procedures

Cylindrical specimens of the Co-27Cr-5Mo alloy with a diameter of 6mm and height of 3mm were prepared for Split Hopkinson Pressure Bar (SHPB) tests. The samples were machined by wire EDM from tibia trays of knee implant samples which were manufactured using investment casting. The chemical composition of the material is shown Table 1 and is in accordance with ISO 5832-4:2014 [33]. The specimens were thermo-mechanically treated using hot isostatic pressing (HIP) and partial solution treatment (PST) to ensure a uniform microstructure as shown in Fig. 1.

Table 1. Chemical composition (in wt%) of the Co-27Cr-5Mo biomedical grade cobalt chromium used

Cr	Mo	Ni	Fe	C	Mn	Si	W	P	S	N	Al	Ti	B	Co
27	5	0.25	0.2	0.22	0.5	0.7	0.01	0.01	0.005	0.15	0.05	0.01	0.006	Bal

Fig. 1. Grains observed in the Co-27Cr-5Mo alloy after HIP and PST.

The SHPB arrangement consisted of a 250 mm long striker bar, 500 mm long incident bar, 500 mm long transmitted bar and a 250 mm long momentum trap bar. All bars had a diameter of 12.7 mm and were made from Inconel 718 alloy. The specimen contact faces were lubricated with dry colloidal graphite. An induction heater with uniform field around the specimen was used to heat the specimen to the desired temperature. The temperature was measured using a thermocouple placed in mechanical contact with the end of the transmitted bar using steel O clips and silver dag. The temperature was not regulated during the experiment as the test duration was 100 µs, leading to negligible heat loss to the surrounding air. Tests were conducted over a wide processing domain of temperatures (298 K, 473 K, 673 K and 873 K) and strain-rates (600 s^{-1}, 1000 $s^{-1,}$ 1400 s^{-1}). The input, reflected and transmitted pulses were measured using photon Doppler velocimetry based methods [34]. Laser light of 1550 nm wavelength was reflected at a shallow angle from the bar surfaces and mixed with un-shifted light. The frequency of the resultant beat pattern was measured as a function of time using GHz response photodiodes and converted to a particle velocity in the direction of firing. A schematic of the SHPB system is shown in Fig. 2. Full details on the SHPB experimental testing set-up can be found in [34].

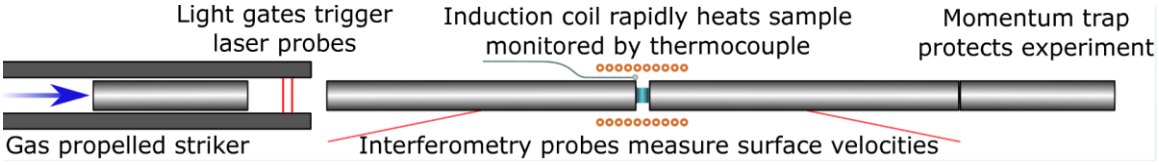

Fig. 2. Schematic of SHPB system.

3. Experimental results

The solution procedures to determine the material constants for the different constitutive models are outlined below. These constants were then used as inputs into a nonlinear least

squares optimisation simulation for further refinement based on the fminsearch routine in Matlab. The following objective function was used to obtain the constants:

$$\phi = \sum_{i}^{n} \left[log(\sigma_{model}) - log\left(\sigma_{exp}\right) \right]^2 \quad (1)$$

where ϕ is the function to minimise, σ_{model} is the predicted flow stress from the model, σ_{exp} is the experimental flow stress. During this analysis, 298K was taken as the reference temperature and 600s^{-1} as the reference strain-rate for all models.

3.1 Modified Zerilli-Armstrong model

The modified Zerilli-Armstrong (ZA) model can be represented as follows [12]:

$$\sigma = (C_1 + C_2\varepsilon^n) exp[-(C_3 + C_4\varepsilon)T^* + (C_5 + C_6T^*) ln\dot{\varepsilon}^*] \quad (2)$$

where σ is the flow stress, ε is the plastic strain, $\dot{\varepsilon}^* = \dot{\varepsilon}/\dot{\varepsilon}_0$ is the dimensionless strain rate with $\dot{\varepsilon}$ being the strain rate and $\dot{\varepsilon}_0$ the reference stain rate, $T^* = \left(T - T_{ref}\right)$ with T being the current temperature and T_{ref} the reference temperature and C_1, C_2, C_3, C_4, C_5 C_6, n are all material constants. At the reference strain rate, Eq.(2) can be represented as follows:

$$\sigma = (C_1 + C_2\varepsilon^n) exp[-(C_3 + C_4\varepsilon)T^*]. \quad (3)$$

Taking the natural logarithm of both sides gives:

$$ln\,\sigma = ln(C_1 + C_2\varepsilon^n) - (C_3 + C_4\varepsilon)T^*. \quad (4)$$

Substituting the experimental flow stress data at $\dot{\varepsilon}$=1 s^{-1} into Eq.(4), the plot of $ln\,\sigma$ against T^* for different strains can be produced as shown in Fig. 3(a). By performing a linear fit at the different strain values, eight values of $-(C_3 + C_4\varepsilon)$ and $ln(C_1 + C_2\varepsilon^n)$ can be gained from the slope and intercept respectively. The intercept of the line represented by Eq.(4) can be represented as:

$$I_1 = ln(C_1 + C_2\varepsilon^n). \quad (5)$$

Taking the natural logarithm of both sides, Eq.(5) can be rearranged as follows:

$$ln(expI_1 - C_1) = lnC_2 + nln\varepsilon \quad (6)$$

Where C_1 is the yield stress of the true stress-strain curve at reference temperature (T=303 K) and strain rate ($\dot{\varepsilon}$=1 s^{-1}). Hence the plot of $ln(expI_1 - C_1)$ against $ln\varepsilon$ can be obtained as shown in Fig. 3(b) and the values of n and C_2 can be calculated from the slope and intercept respectively by performing a linear fit. Similarly, the slope of the line represented by Eq.(4) can be represented as:

$$S_1 = -(C_3 + C_4\varepsilon). \quad (7)$$

The plot of S_1 against ε can be obtained as shown in Fig. 3(c), hence the values C_3 and C_4 can be calcualted from the intercept and slope respectively by performing a linear fit. Taking the natural logarithm of both sides and rearranging, Eq.(2) can be expressed as:

$$\ln\sigma = \ln(C_1 + C_2\varepsilon^n) - (C_3 + C_4\varepsilon)T^* + (C_5 + C_6T^*)ln\dot{\varepsilon}^*. \quad (8)$$

From the plot of $\ln\sigma$ against $ln\dot{\varepsilon}^*$, five values of $(C_5 + C_6T^*)$ can be obtained from the slope S_2 for the five different temperatures. Hence, S_2 can be represented as follows:

$$S_2 = C_5 + C_6T^*. \quad (9)$$

From the plot S_2 against T^* as shown in Fig. 3(d), C_5 and C_6 are obtained from the intercept and slope respectively. Eleven sets of C_5 and C_6 are obtained at different strains. A constrained optimised procedure is done by minimising the average absolute relative error (AARE) between experimental and predicted flow stress. Hence, all the material constants of the modified ZA equation are calculated and given in Table 2, thus the constitutive equation can be obtained as follows:

$$\sigma = (474.02 + 189.19\varepsilon^{0.2505})exp[-(3.074E^{-4} - 0.00157\varepsilon)T^* + (0.438 - 4.99E^{-4}T^*)ln\dot{\varepsilon}^*]. \quad (10)$$

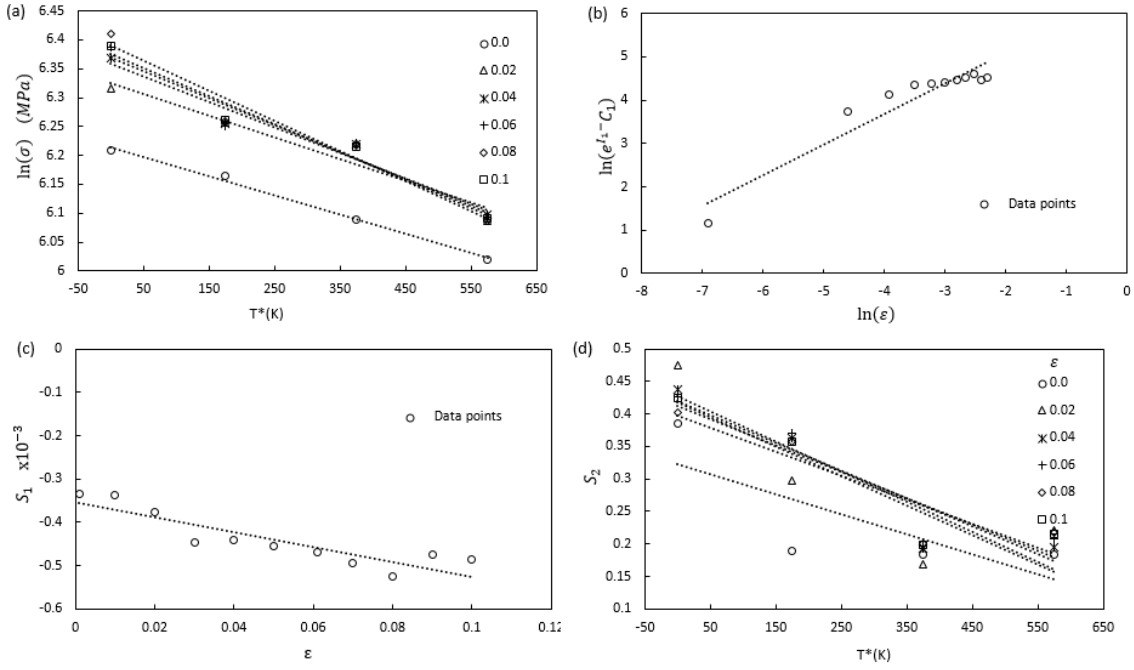

Fig. 3. Plot of (a) $ln\ \sigma$ against T^* at reference strain-rate of $\dot{\varepsilon}$=1 s^{-1}, (b) Plot of $ln(expI_1 - C_1)$ against $ln\varepsilon$, (c) Plot of S_1 against ε and (d) S_2 against T^*

Table 2. Parameters for the modified ZA model

Constant	C_1 (MPa)	C_2 (MPa)	C_3	C_4	C_5	C_6	n
Initial	496.69	657.21	$3.53E^{-4}$	0.0017	0.4022	$-4.67E^{-4}$	0.7027
Optimised	474.02	189.19	$3.074E^{-4}$	0.00157	0.438	$-4.99E^{-4}$	0.2505

Using the optimised parameters summarised in Table 2, the flow stress data is predicted over various processing conditions. Comparisons between the experimental and predicted data by the modified ZA model is shown in Fig. 4.

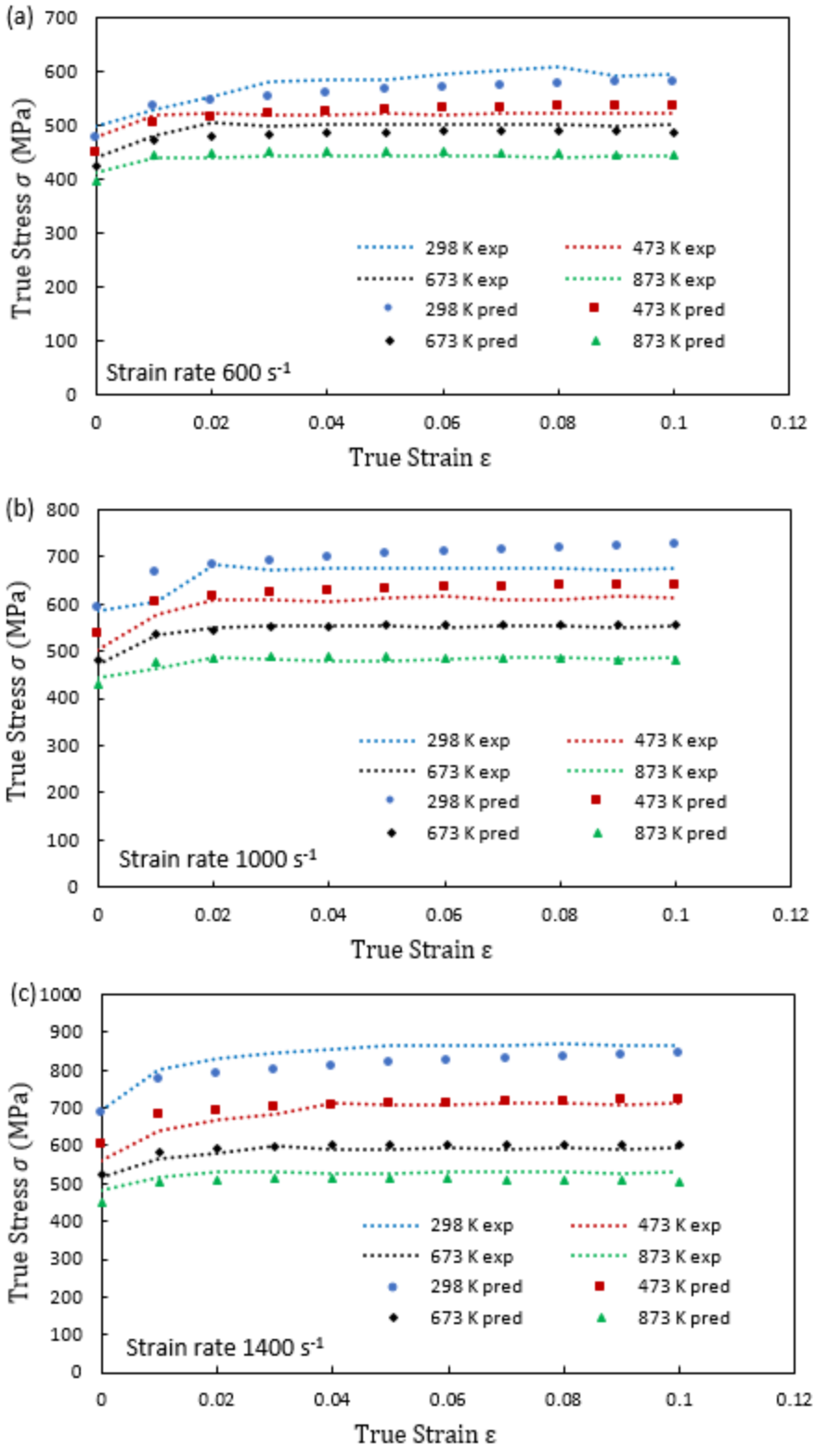

Fig. 4. Comparison between experimental and predicted flow stress values by the modified *ZA* model at a strain rate of (a) 600 s^{-1}, (b) 1000 s^{-1} and (c) 1400 s^{-1}

3.2 Modified Johnson-Cook model

The modified Johnson-Cook (JC) model can represented as follows [18]:

$$\sigma = (A_1 + B_1\varepsilon + B_2\varepsilon^2)(1 + C_1 ln\dot{\varepsilon}^*)exp[(\lambda_1 + \lambda_2 ln\dot{\varepsilon}^*)T^*] \quad (11)$$

Where σ is the flow stress, A_1, B_1, B_2, λ_1, λ_2 are all material constants, ε is the plastic strain, $\dot{\varepsilon}^* = \dot{\varepsilon}/\dot{\varepsilon}_0$ is the dimensionless strain rate with $\dot{\varepsilon}$ being the strain rate and $\dot{\varepsilon}_0$ the reference strain rate, $T^* = (T - T_{ref})$ with T being the current temperature and T_{ref} the reference temperature. At reference temperature and strain rate, Eq.(11) reduces to:

$$\sigma = (A_1 + B_1\varepsilon + B_2\varepsilon^2). \quad (12)$$

By substituting the corresponding flow stress and strain data into Eq.(12) and plotting the graph of σ against ε, the values of A_1, B_1 and B_2 can be calculated by performing a two-order polynomial fit as shown in Fig. 5(a). At the reference temperature, Eq.(11) can be expressed as:

$$\frac{\sigma}{(A_1 + B_1\varepsilon + B_2\varepsilon^2)} = 1 + C_1 ln\dot{\varepsilon}^* \quad (13)$$

hence, C_1 can be calculated from the slope of $\sigma/(A_1 + B_1\varepsilon + B_2\varepsilon^2)$ against $ln\dot{\varepsilon}^*$ as shown in Fig. 5(b) by performing a linear fit. By introducing a new parameter λ, where λ=$\lambda_1 + \lambda_2 ln\dot{\varepsilon}^*$, Eq.(11) can be expressed as:

$$\frac{\sigma}{(A_1 + B_1\varepsilon + B_2\varepsilon^2)(1 + C_1 ln\dot{\varepsilon}^*)} = e^{\lambda T^*} \quad (14)$$

thus, by multiplying each side by the natural logarithm, Eq.(14) can be rearranged as follows:

$$ln\left\{\frac{\sigma}{(A_1 + B_1\varepsilon + B_2\varepsilon^2)(1 + C_1 ln\dot{\varepsilon}^*)}\right\} = \lambda T^*. \quad (15)$$

Plots of $ln\{\sigma/(A_1 + B_1\varepsilon + B_2\varepsilon^2)(1 + C_1 ln\dot{\varepsilon}^*)\}$ against T^* over the entire processing range of temperature, strain and strain rate give three values of λ for each of the three strain rates by performing a linear fit and calculating the slope as shown in Fig. 5(c). As λ is a function of strain rate, λ_1 and λ_2 can be calculated from the plot λ against $ln\dot{\varepsilon}^*$ as the intercept and slope respectively by performing a linear fit as shown in Fig. 5(d).The material constants of the modified JC equation are shown in Table 3 and the constitutive equation can be obtained as follows:

$$\sigma = (504.19 + 2182.46\varepsilon - 16223.1\varepsilon^2)(1 + 0.5068 ln\dot{\varepsilon}^*)exp[(-4.0957E^{-4} - 4.609E^{-4} ln\dot{\varepsilon}^*)T^*]. \quad (16)$$

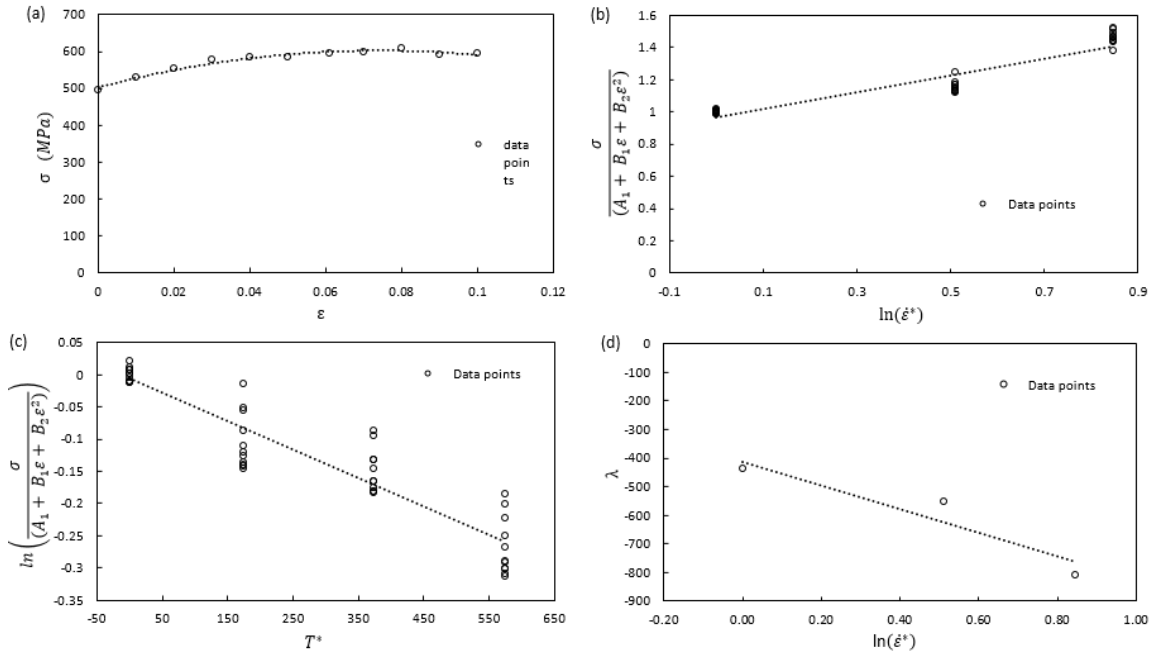

Fig. 5. Plot of (a) σ against ε at reference strain-rate and temperature, (b) $\sigma/(A_1 + B_1\varepsilon + B_2\varepsilon^2)$ against $ln\dot{\varepsilon}^*$, (c) $ln\{\sigma/(A_1 + B_1\varepsilon + B_2\varepsilon^2)(1 + C_1 ln\dot{\varepsilon}^*)\}$ against $ln\dot{\varepsilon}^*$ at reference strain-rate and (d) λ against $ln\dot{\varepsilon}^*$.

Table 3. Parameters for the modified JC model

Constant	A_1	B_1	B_2	C_1	λ_1	λ_2
Initial	502.93	2692.56	-1816.11	0.5219	$-4.114E^{-4}$	$-4.175E^{-4}$
Optimised	504.19	2182.46	-16223.1	0.506812	$-4.0957E^{-4}$	$-4.6056E^{-4}$

Using the optimised constants summarised in Table 3, the flow stress data is predicted for various processing conditions. Comparisons between the experimental and predicted data by the modified JC model is shown in Fig. 6.

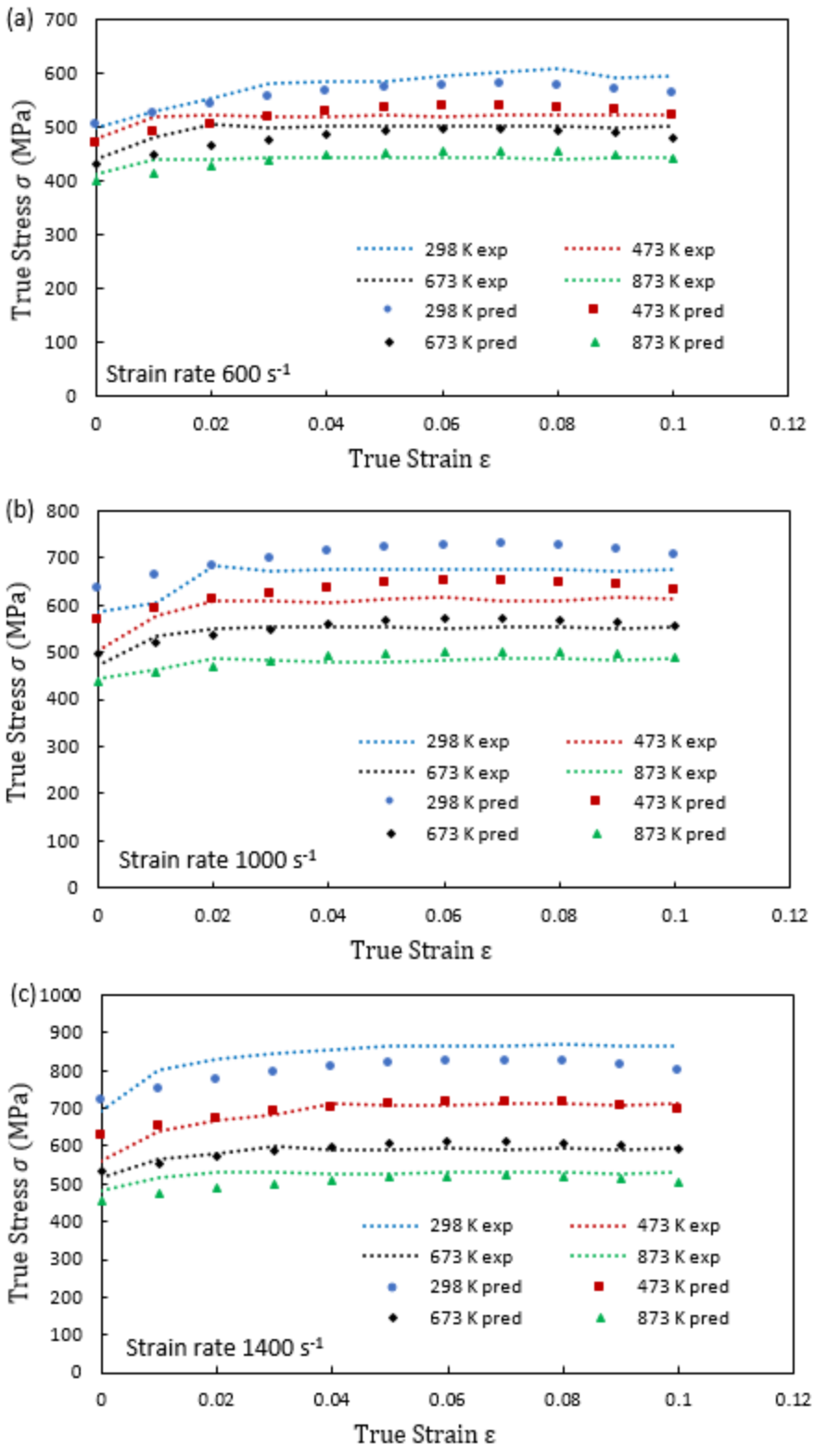

Fig. 6. Comparison between experimental and predicted flow stress values by the modified *JC* model at a strain rate of (a) 600 s^{-1}, (b) 1000 s^{-1} and (c) 1400 s^{-1}

3.3. Arrhenius-type model

The effects of temperature and strain rate on deformation behaviour can be represented by the Zener-Holloman parameter (Z) in an exponent-type equation expressed as [29]:

$$Z = \dot{\varepsilon} exp\left(\frac{Q}{RT}\right) \tag{17}$$

where $\dot{\varepsilon}$ is the strain rate (s^{-1}), R (8.31 $Jmol^{-1}K^{-1}$) is the universal gas constant, T is the temperature (K) and Q is the activation energy of hot deformation (KJ mol^{-1}). The Arrhenius-type equation, which gives the relationship between flow stress and Z can be expressed as [35]:

$$\dot{\varepsilon} = AF(\sigma) exp\left(\frac{-Q}{RT}\right) \tag{18}$$

$$F(\sigma) = \begin{Bmatrix} \sigma^{n_1}, & \alpha\sigma < 0.8 \\ exp(\beta\sigma), & \alpha\sigma > 1.2 \\ [sinh(\alpha\sigma)]^n, & for\ all\ \sigma \end{Bmatrix}$$

where σ is the flow stress (MPa) for a given strain, α, n_1, n, A and β are material constants, $\alpha = \beta/n_1$. In this investigation, the strain of 0.0 was taken as an example to introduce the solution procedures of determining the material constants. For low stress levels ($\alpha\sigma < 0.8$) and high stress levels ($\alpha\sigma > 1.2$), substituting the power law and exponential law of $F(\sigma)$ into Eq.(18) yields the following:

$$\dot{\varepsilon} = B\sigma^{n_1} \tag{19}$$

$$\dot{\varepsilon} = Cexp(\beta\sigma) \tag{20}$$

where B and C are material constants. Taking the natural logarithm of both sides of Eq.(19) and Eq.(20), respectively, gives:

$$ln(\sigma) = \frac{1}{n_1} ln(\dot{\varepsilon}) - \frac{1}{n_1} ln(B) \tag{21}$$

$$\sigma = \frac{1}{\beta} ln(\dot{\varepsilon}) - \frac{1}{\beta} ln(C). \tag{22}$$

By substituting the values of flow stress and corresponding strain rate under the strain of 0.0 for all deformation temperatures into Eq.(21) and Eq.(22), values for n_1 and β can be calculated from the slope of the plots $ln(\sigma)$ against $ln(\dot{\varepsilon})$ and σ against $ln(\dot{\varepsilon})$ respectively as shown in Fig. 7(a) and Fig. 7(b) respectively. The average slope values for the different temperatures are taken when calculating n_1 and β. Then, the corresponding value of $\alpha = \beta/n_1$ can be calculated. When considering all stress levels, Eq.(18) can be expressed as:

$$\dot{\varepsilon} = A[sinh(\alpha\sigma)]^n exp\left(\frac{-Q}{RT}\right). \tag{23}$$

Taking the natural logarithm of both sides and rearranging, Eq. (23) can be expressed as:

$$ln[sinh(\alpha\sigma)] = \frac{ln\dot{\varepsilon}}{n} + \frac{Q}{nRT} - \frac{lnA}{n}. \tag{24}$$

By substituting the values of flow stress and corresponding strain rate under the strain of 1.0 for all deformation temperatures into Eq.(24), the value for n can be calculated from the average slope in the plot of $ln[sinh(\alpha\sigma)]$ against $ln(\dot{\varepsilon})$ as shown in Fig. 7(c). By differentiating Eq.(24), the following formula can be derived for a particular strain rate:

$$Q = 100Rn\frac{d\{ln[sinh(\alpha\sigma)]\}}{d(1000/T)}. \quad (25)$$

The value Q can be calculated from the average slope of the plot $ln[sinh(\alpha\sigma)]$ against $1000/T$ under different strain rates as shown in Fig. 7(d). Hence, the value of A can be calculated from the intercept of the plot $ln[sinh(\alpha\sigma)]$ against $ln(\dot{\varepsilon})$.

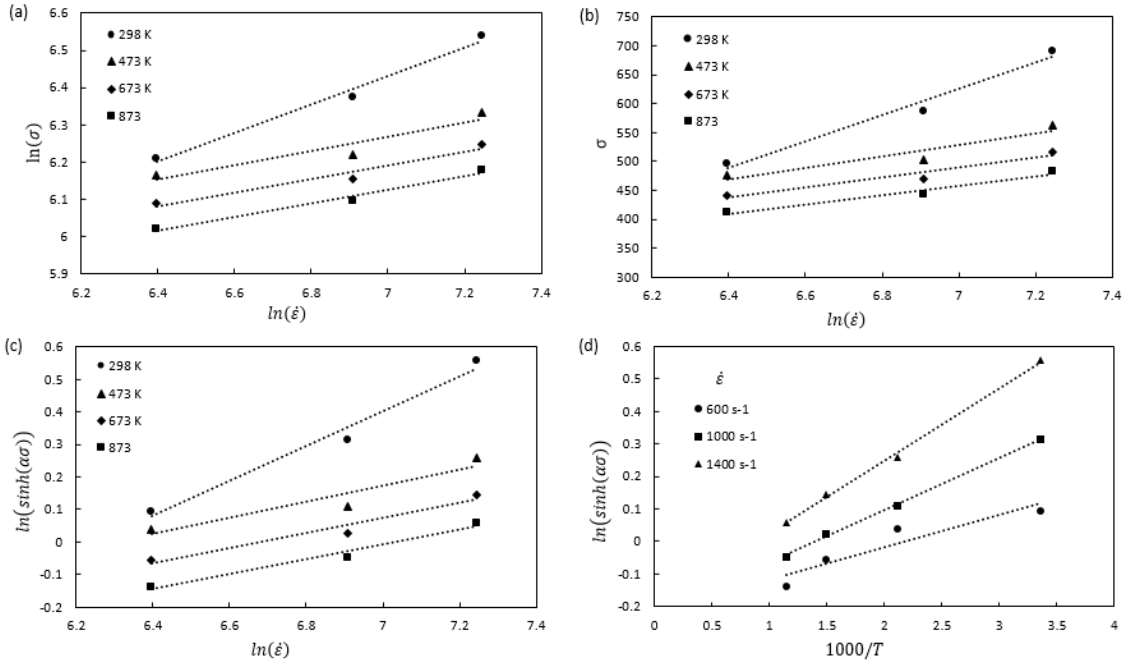

Fig. 7. Plots of (a) $ln(\sigma)$ against $ln(\dot{\varepsilon})$, (b) σ against $ln(\dot{\varepsilon})$, (c) $ln[sinh(\alpha\sigma)]$ against $ln(\dot{\varepsilon})$ and (d) $ln[sinh(\alpha\sigma)]$ against $1000/T$ at 0.0 strain

The influence of strain on flow stress behaviour is assumed to be insignificant in Eq.(17) and Eq.(18). However, experimental results indicate a variation of stress with strain. Hence, it is necessary to use a method of strain compensation. The influence of strain in the constitutive equation is incorporated by assuming that the material constants are polynomial functions of strain. A 2nd order polynomial, as shown in Eq.(26), was found to represent the influence of strain with material constants with good correlation and generalisation as shown in Fig. 8. The coefficients of the polynomial are given in Table 4.

$$\alpha = \alpha_1\varepsilon^2 + \alpha_2\varepsilon + \alpha_3$$
$$n = n_1\varepsilon^2 + n_2\varepsilon + n_3$$
$$Q = Q_1\varepsilon^2 + Q_2\varepsilon + Q_3 \quad (26)$$
$$A = A_1\varepsilon^2 + A_2\varepsilon + A_3$$

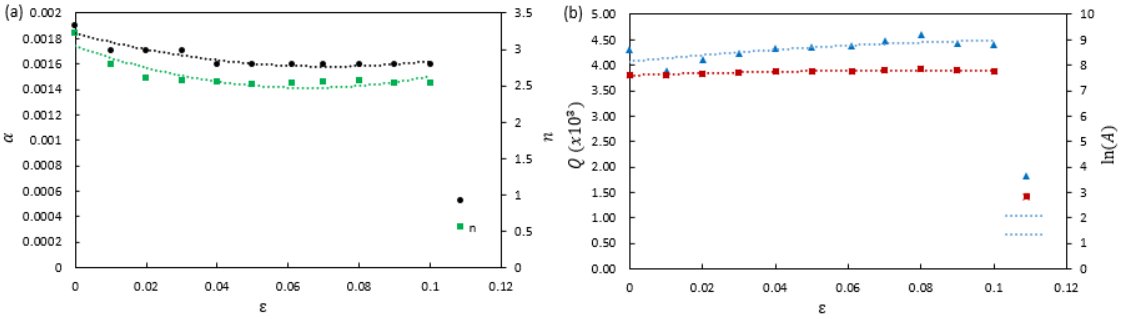

Fig. 8. Variation of (a) α and n, (b) Q and lnA with true strain

Table 4. Polynomial coefficients for α, n, Q and lnA

i	α_i (initial)	α_i (optimised)	n_i (initial)	n_i (optimised)	Q_i (initial)	Q_i (optimised)	$(lnA)_i$ (initial)	$(lnA)_i$ (optimised)
1	0.0534	0.0084	134.575	162.20	-27291.80	-28485.4	-28.847	403.9834
2	-0.0071	-1.42E^{-5}	-17.622	-21.575	6858.74	6713.425	4.801	-84.3168
3	0.0018	7.69E^{-5}	3.0475	3.867	4076.52	3945.39	7.602	20.245

According to the definition of hyperbolic law, the flow stress can be written as a function of the Zener-Hollomon parameter as shown in Eq.(27). The comparison between the experimental and predicted data from the strain compensated Arrhenius-type constitutive equation at various processing conditions is shown in Fig. 9.

$$\sigma = \frac{1}{\alpha} ln\left\{\left(\frac{Z}{A}\right)^{1/n} + \left[\left(\frac{Z}{A}\right)^{2/n} + 1\right]^{1/2}\right\} \quad (27)$$

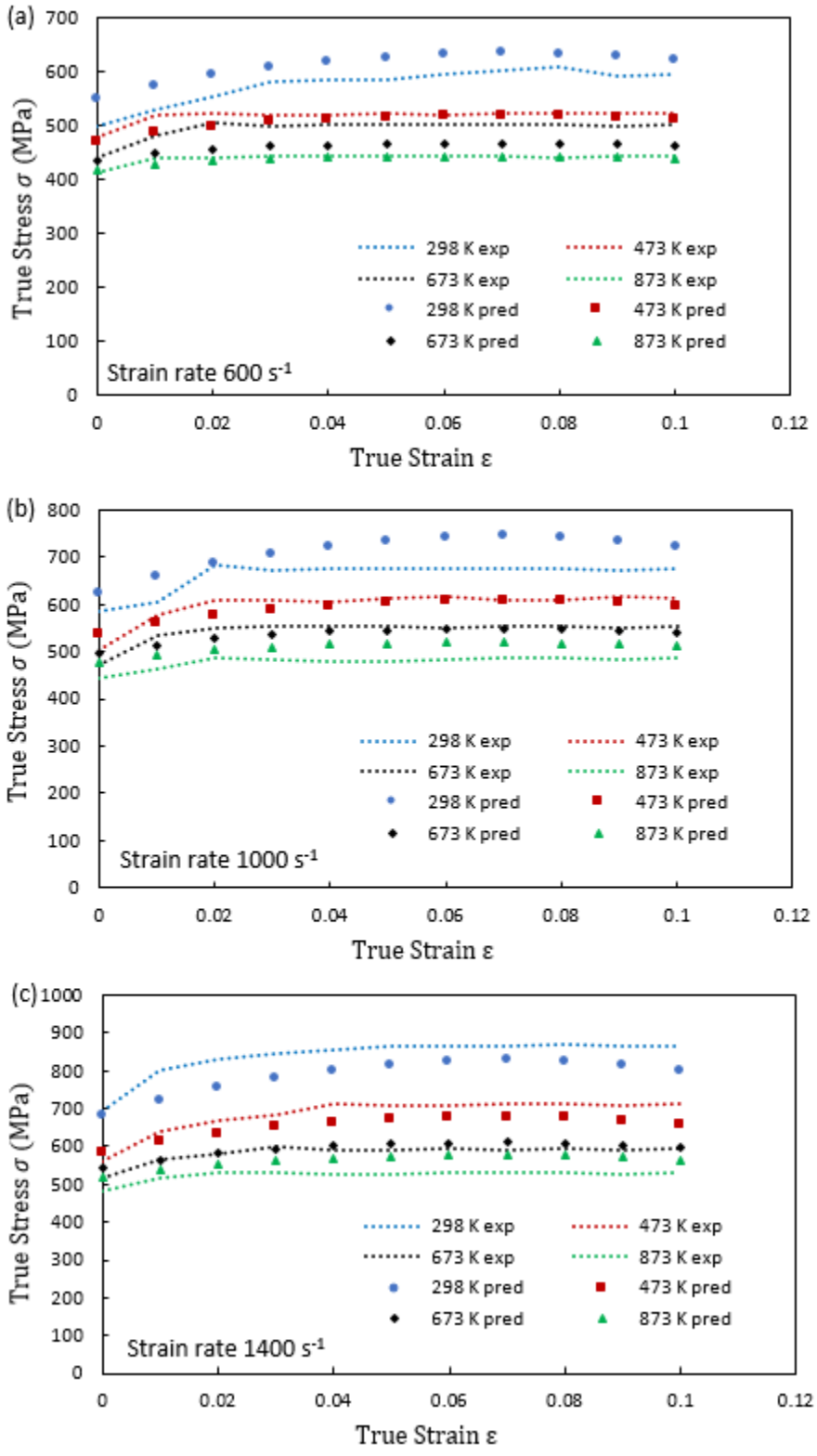

Fig. 9. Comparison between experimental and predicted flow stress values by the strain compensated Arrhenius-type model at a strain rate of (a) 600 s^{-1}, (b) 1000 s^{-1} and (c) 1400 s^{-1}

4. Discussion

In order to make a comparative analysis on the predictability of the three models, the correlation coefficient (*R*) and the average absolute relative error (*AARE*) were used to evaluate the deviation of the predicted flow stresses. The correlation coefficient (*R*) provides information on the strength of the linear relationship between the experimental and predicted values. It should be noted that a higher value of *R* may not necessarily indicate better performance due to the tendency of the model to be biased towards higher or lower values [16]. However, the average absolute relative error (*AARE*) is computed through a term by term comparison of the relative error and is therefore an unbiased statistical parameter for measuring the predictability of a model. The correlation coefficient (*R*) and average absolute relative error (*AARE*) can be expressed as:

$$R = \frac{\sum_{i=1}^{N}(E_i - \bar{E})(P_i - \bar{P})}{\sqrt{\sum_{i=1}^{N}(E_i - \bar{E})^2 \sum_{i=1}^{N}(P_i - \bar{P})^2}} \tag{28}$$

$$AARE(\%) = \frac{1}{N}\sum_{i=1}^{N}\left|\frac{E_i - P_i}{E_i}\right| x100 \tag{29}$$

where E_i is the experimental data and P_i is the predicted data, $\bar{E}$ and $\bar{P}$ are the mean experimental and predicted values respectively, and N is the total number of data employed in the analysis. Comparison of the correlation coefficient and average absolute relative error for the three different models (*MZA, MJC, AT*) is displayed in Fig. 10. The modified *ZA* model recorded the highest correlational coefficient and lowest absolute relative error compared to the other models and hence is most suitable to predict the flow stress behaviour of biomedical grade *Co-27Cr-5Mo* at high strain rates. This can be attributed to the ability of the model to predict coupled effects between strain, strain rate and temperature. For example, within the *AT* model, the Zener-Holloman parameter (Z) shown in Eq. (17) considers the coupled effect of strain rate and temperature. However, only one material constant *Q* is used to represent this coupled effect. Within the modified *JC* model, the first term ($A_1 + B_1\varepsilon + B_2\varepsilon^2$) represents the effect of strain hardening, the second terms ($1 + C_1 ln\dot{\varepsilon}^*$) represents the effect of strain rate hardening and the third term ($exp[(\lambda_1 + \lambda_2 ln\dot{\varepsilon}^*)T^*]$) represents the coupled effect of strain rate and temperature. This coupled effect is represented by two material constants (λ_1 and λ_2) and hence the model has a greater prediction capability compared to the strain compensated *AT* model. Within the modified *ZA* model the first term ($C_1 + C_2\varepsilon^n$) is used to describe the effect of strain hardening. The second term ($exp[-(C_3 + C_4\varepsilon)T^* + (C_5 + C_6T^*)ln\dot{\varepsilon}^*]$) can be broken down into two separate components. The $(C_5 + C_6T^*)ln\dot{\varepsilon}^*$ component represents the coupled effect of temperature and strain rate. Similar to the modified *JC* model two material constants are used to represent this effect. The $(-(C_3 + C_4\varepsilon)T^*)$ component represents the coupled effect of strain and temperature. It is the addition of this second coupled effect that leads to greater predictability with the modified *ZA* model. A comparison of different *R* and *AARE* values recorded for different materials, models and processing conditions is shown in Table 5. Similar results of the modified *ZA* demonstrating greater predictability were shown by Samantaray et al [12,16] and also Gupta et al [36].

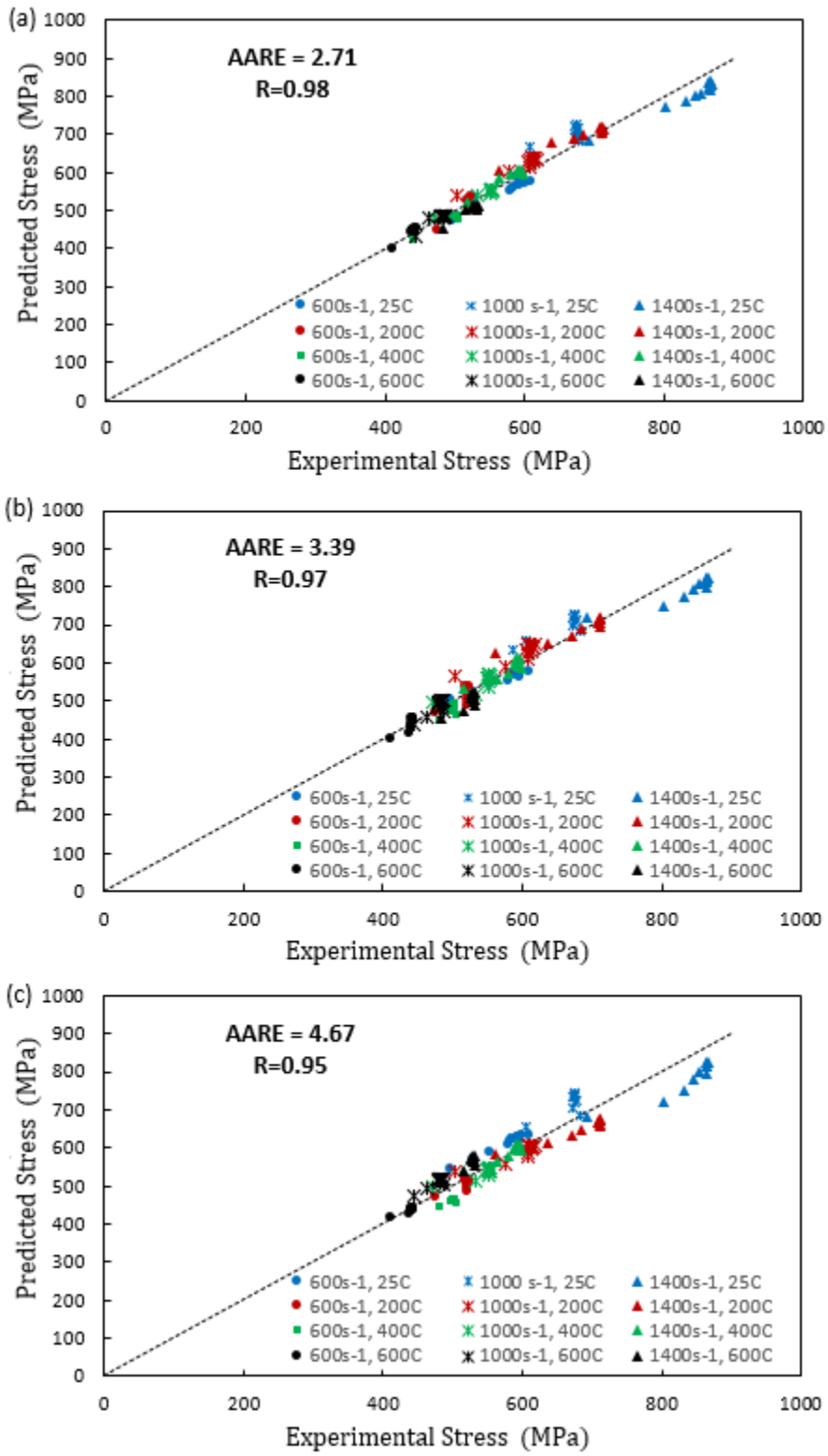

Fig. 10. Correlation between experimental and predicted flow stress values for (a) modified Zerilli-Armstrong model, (b) modified Johnson-Cook model and (c) strain-compensated Arrhenius-type model.

Table 5. Comparison of *R* and *AARE* for different materials, models and processing conditions

Material	Temperature (K)	Strain Rate (s^{-1})	Testing Method	Model	Correlation Coefficient (R)	Absolute Error (%)	Ref
T24 steel	1323-1473	0.01-10	Gleeble 3500	JC MJC	0.962 0.991	9.41 5.37	[10]
Titanium modified austenitic stainless steel (Alloy D9)	1073-1473	0.001-1	Servo-hydraulic	JC MZA	0.916 0.995	17 5.3	[12]
9 Cr-1Mo steel	1123-1373	0.001-1	Servo-hydraulic	JC MZA AT	0.977 0.992 0.989	26 5.7 5.87	[16]
20CrMo alloy steel	1173-1373	0.0015-0.015	Gleeble 1500	JC MJC AT	0.86 0.97 0.98	19.9 8.8 8.4	[22]
OFHC copper, Vanadium and α-titanium	300-1100	4000	Kolsky bar	ZA	-	10.2	[25]
28CrMnMoV steel	1173-1473	0.01-10	Gleeble 3500	MJC MZA ATC	0.992 0.989 0.991	5.34 5.76 5.07	[37]
Austenitic stainless steel 316	323-623	0.0001-0.1	UTM	JC MZA ATC ANN	0.942 0.987 0.985 0.993	6.63 3.32 3.34 1.25	[36]
12Cr3Wv steel	1223-1373	0.1-30	Gleeble 1500	ATC ANN	0.995 0.999	3.48 0.58	[38]
2024Al-T3 Alloy	573-773	0.001-100	Gleeble-3800	JC MJC AT ATC	0.9768 0.9873 0.9872 0.9882	25.09 7.93 7.08 6.41	[39]
AA7075	523-723	0.001-100	Gleeble-3800	MJC MZA AT	0.9752 0.9723 0.9775	7.75 8.36 6.68	[40]
CoCr	298-873	600-1400	SHPB	MZA MJC ATC	0.985 0.972 0.954	2.71 3.39 4.67	-

Particularly high values of *AARE* were recorded at room temperature (298 K) for both the modified *ZA* model and the modified *JC* model compared to other temperatures as shown in Fig. 11. High values of *AARE* were also recorded for the *AT* model at room temperature but this was similar for all temperatures. Tests conducted at room temperature were used as the reference temperature (T_{ref}) when calculating the constants for both the modified *ZA* model and modified *JC* model. At reference temperature, the modified *ZA* model is reduced significantly to

$$\sigma = (C_1 + C_2\varepsilon^n)exp[C_5 ln\dot{\varepsilon}^*]. \quad (30)$$

The second term of the model $[-(C_3 + C_4\varepsilon)T^*]$ and $[C_6T^*]$ from the third term reduce to zero leaving only three constants. The first term $(C_1 + C_2\varepsilon^n)$ represents the yield strength and strain hardening. This term gives the initial shape to the stress-strain curve. The remainder of third term $exp[C_5 ln\dot{\varepsilon}^*]$ represents the shift of the curve at different strain-rates. Hence, only one constant, C_5, influences this shift at different strain-rates. The nonlinear least squares optimisation procedure will try to balance this one constant for different strain-rates at the reference temperature to achieve an overall low value of *AARE*. The average stress at reference temperature is 595, 674 and 846 MPa at strain-rates 600, 1000 and 1400 s^{-1} respectively. There is a large variation in average stress at different strain-rates at the reference temperature. Hence, using only one constant in a term to represent this large variation in stress results in higher AARE values at these conditions. Similarly, at reference temperature, the modified *JC* model is reduced significantly to:

$$\sigma = (A_1 + B_1\varepsilon + B_2\varepsilon^2)(1 + C_1 ln\dot{\varepsilon}^*). \quad (31)$$

Again, only one constant, C_1, influences the shift of the stress-strain curve at different strain-rates which results in higher values of *AARE* at reference temperature.

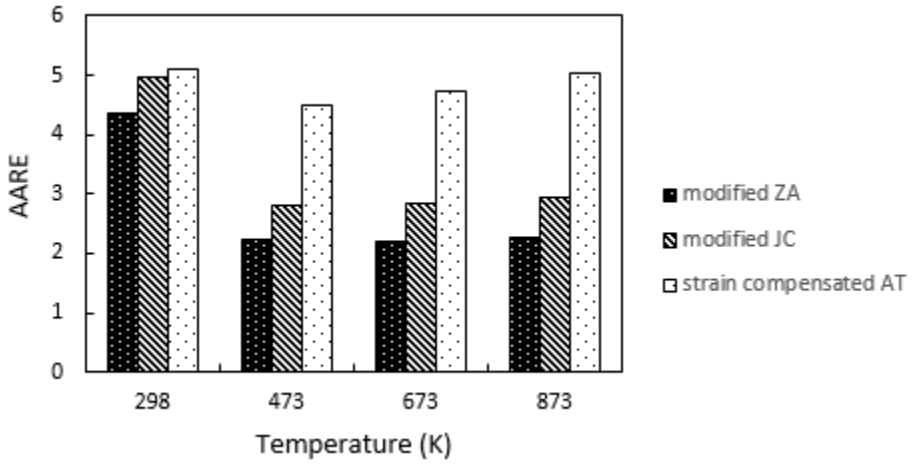

Fig. 11. Difference in AARE at different temperatures for three models

5. Conclusions

In this paper, a comparative study has been made on the ability of the modified Zerilli-Armstrong, modified Johnson-Cook and strain compensated Arrhenius-type models to predict

the high strain rate deformational flow behaviour of biomedical grade *Co-27Cr-5Mo* alloy using statistical parameters such as correlation coefficient (R) and Average Absolute Relative Error (AARE). The modified Zerilli-Armstrong model recorded the lowest AARE (2.71%) and highest correlation coefficient (R=0.98) compared to the other models and is therefore most suitable to predict the flow stress behaviour of biomedical grade *Co-27Cr-5Mo* at high strain rates. This greater predictability was attributed to the model representing the coupling effect of temperature with strain rate and also temperature with strain.

6. Acknowledgements

This work was funded and supported by the Irish Research Council (*IRC*). Split Hopkinson Pressure Bar tests were conducted at The Cavendish Laboratory, University of Cambridge, United Kingdom.

7. References

[1] D. Granchi, G. Ciapetti, S. Stea, L. Savarino, F. Filippini, a Sudanese, G. Zinghi, L. Montanaro, Cytokine release in mononuclear cells of patients with Co-Cr hip prosthesis., Biomaterials. 20 (1999) 1079–1086. doi:10.1016/s0142-9612(99)00004-6.

[2] D.R. Haynes, T.N. Crotti, M.R. Haywood, Corrosion of and changes in biological effects of cobalt chrome alloy and 316L stainless steel prosthetic particles with age, J. Biomed. Mater. Res. 49 (2000) 167–175. doi:10.1002/(SICI)1097-4636(200002)49:2<167::AID-JBM3>3.0.CO;2-9.

[3] J. Keller, Lautenschlager EP, Handbook of biomaterials evaluation, New York, 1986.

[4] Y.B. Guo, An integral method to determine the mechanical behavior of materials in metal cutting, J. Mater. Process. Technol. 142 (2003) 72–81. doi:10.1016/S0924-0136(03)00462-X.

[5] A. Shokrani, V. Dhokia, S.T. Newman, Investigation of the effects of cryogenic machining on surface integrity in CNC end milling of Ti-6Al-4V titanium alloy, J. Manuf. Process. 21 (2016) 172–179. doi:10.1016/j.jmapro.2015.12.002.

[6] J.H. Sung, J.H. Kim, R.H. Wagoner, A plastic constitutive equation incorporating strain, strain-rate, and temperature, Int. J. Plast. 26 (2010) 1746–1771. doi:10.1016/j.ijplas.2010.02.005.

[7] R. Liu, M. Salahshoor, S.N. Melkote, T. Marusich, A unified material model including dislocation drag and its application to simulation of orthogonal cutting of OFHC Copper, J. Mater. Process. Technol. 216 (2015) 328–338. doi:10.1016/j.jmatprotec.2014.09.021.

[8] Y.C. Lin, M.S. Chen, J. Zhang, Modeling of flow stress of 42CrMo steel under hot compression, Mater. Sci. Eng. A. 499 (2009) 88–92. doi:10.1016/j.msea.2007.11.119.

[9] Y. Han, G. Qiao, J. Sun, D. Zou, A comparative study on constitutive relationship of as-cast 904L austenitic stainless steel during hot deformation based on Arrhenius-

type and artificial neural network models, Comput. Mater. Sci. 67 (2013) 93–103. doi:10.1016/j.commatsci.2012.07.028.
[10] H.Y. Li, X.F. Wang, J.Y. Duan, J.J. Liu, A modified Johnson Cook model for elevated temperature flow behavior of T24 steel, Mater. Sci. Eng. A. 577 (2013) 138–146. doi:10.1016/j.msea.2013.04.041.
[11] P.S. Follansbee, U.F. Kocks, A constitutive description of the deformation of copper based on the use of the mechanical threshold stress as an internal state variable, Inst. Phys. Conf. Ser. 102 (1989) 237–244.
[12] D. Samantaray, S. Mandal, U. Borah, A.K. Bhaduri, P. V. Sivaprasad, A thermo-viscoplastic constitutive model to predict elevated-temperature flow behaviour in a titanium-modified austenitic stainless steel, Mater. Sci. Eng. A. 526 (2009) 1–6. doi:10.1016/j.msea.2009.08.009.
[13] Y.C. Lin, X.-M. Chen, A critical review of experimental results and constitutive descriptions for metals and alloys in hot working, Mater. Des. 32 (2011) 1733–1759. doi:http://dx.doi.org/10.1016/j.matdes.2010.11.048.
[14] G.R. Johnson, W.H. Cook, A constitutive model and data for metals subjected to large strains, high strain rates and high temperatures, Proc. 7th Int. Symp. Ballist. 547 (1983) 541–547. doi:10.1038/nrm3209.
[15] F.J. Zerilli, R.W. Armstrong, Dislocation-mechanics-based constitutive relations for material dynamics calculations, J. Appl. Phys. 61 (1987) 1816–1825. doi:10.1063/1.338024.
[16] D. Samantaray, S. Mandal, A.K. Bhaduri, A comparative study on Johnson Cook, modified Zerilli-Armstrong and Arrhenius-type constitutive models to predict elevated temperature flow behaviour in modified 9Cr-1Mo steel, Comput. Mater. Sci. 47 (2009) 568–576. doi:10.1016/j.commatsci.2009.09.025.
[17] A. Rusinek, J.A. Rodríguez-Martínez, A. Arias, A thermo-viscoplastic constitutive model for FCC metals with application to OFHC copper, Int. J. Mech. Sci. 52 (2010) 120–135. doi:10.1016/j.ijmecsci.2009.07.001.
[18] Y.C. Lin, X.M. Chen, G. Liu, A modified Johnson-Cook model for tensile behaviors of typical high-strength alloy steel, Mater. Sci. Eng. A. 527 (2010) 6980–6986. doi:10.1016/j.msea.2010.07.061.
[19] W. Song, J. Ning, X. Mao, H. Tang, A modified Johnson-Cook model for titanium matrix composites reinforced with titanium carbide particles at elevated temperatures, Mater. Sci. Eng. A. 576 (2013) 280–289. doi:10.1016/j.msea.2013.04.014.
[20] D.-T. Nguyen, T.-L. Banh, D.-W. Jung, S.-H. Yang, Y.-S. Kim, A modified Johnson-Cook model to predict stress-strain curves of boron steel sheets at elevated and cooling temperatures, High Temp. Mater. Process. 31 (2012).
[21] Y.C. Lin, X.M. Chen, A combined Johnson-Cook and Zerilli-Armstrong model for hot compressed typical high-strength alloy steel, Comput. Mater. Sci. 49 (2010) 628–633. doi:10.1016/j.commatsci.2010.06.004.
[22] A. He, G. Xie, H. Zhang, X. Wang, A comparative study on Johnson-Cook, modified Johnson-Cook and Arrhenius-type constitutive models to predict the high temperature flow stress in 20CrMo alloy steel, Mater. Des. 52 (2013) 677–685. doi:10.1016/j.matdes.2013.06.010.

[23] D.N. Zhang, Q.Q. Shangguan, C.J. Xie, F. Liu, A modified Johnson-Cook model of dynamic tensile behaviors for 7075-T6 aluminum alloy, J. Alloys Compd. 619 (2015) 186–194. doi:10.1016/j.jallcom.2014.09.002.
[24] H. Zhan, G. Wang, D. Kent, M. Dargusch, Constitutive modelling of the flow behaviour of a β titanium alloy at high strain rates and elevated temperatures using the Johnson-Cook and modified Zerilli-Armstrong models, Mater. Sci. Eng. A. 612 (2014) 71–79. doi:10.1016/j.msea.2014.06.030.
[25] A.M. Lennon, K.T. Ramesh, The influence of crystal structure on the dynamic behavior of materials at high temperatures, Int. J. Plast. 20 (2004) 269–290. doi:10.1016/S0749-6419(03)00037-8.
[26] J.J. Jonas, C.M. Sellars, W.J.M. Tegart, Strength and structure under hot-working conditions, Int. Mater. Rev. 14 (1969) 1–24. doi:10.1179/095066069790138056.
[27] S. Mandal, V. Rakesh, P. V. Sivaprasad, S. Venugopal, K. V. Kasiviswanathan, Constitutive equations to predict high temperature flow stress in a Ti-modified austenitic stainless steel, Mater. Sci. Eng. A. 500 (2009) 114–121. doi:10.1016/j.msea.2008.09.019.
[28] Y. Wang, J. Peng, L. Zhong, F. Pan, Modeling and application of constitutive model considering the compensation of strain during hot deformation, J. Alloys Compd. 681 (2016) 455–470. doi:10.1016/j.jallcom.2016.04.153.
[29] C. Zener, J.H. Hollomon, Effect of strain rate upon plastic flow of steel, J. Appl. Phys. 15 (1944) 22–32. doi:10.1063/1.1707363.
[30] F.A. Slooff, J. Zhou, J. Duszczyk, L. Katgerman, Constitutive analysis of wrought magnesium alloy Mg-Al4-Zn1, Scr. Mater. 57 (2007) 759–762. doi:10.1016/j.scriptamat.2007.06.023.
[31] Y.C. Lin, M.-S. Chen, J. Zhong, Constitutive modeling for elevated temperature flow behavior of 42CrMo steel, Comput. Mater. Sci. 42 (2008) 470–477. doi:10.1016/j.commatsci.2007.08.011.
[32] S.-R. Chen, C.-Y. Wu, Y.-L. Yeh, Y.-L. Ou, Hot Deformation Resistance of an AA5083 Alloy under High Strain Rates, China Steel Tech. Rep. (2014) 83–88.
[33] BSI Standards Publication Implants for surgery — polyethylene Part 2 : Moulded forms, (2011).
[34] L.J. Lea, A.P. Jardine, Application of photon Doppler velocimetry to direct impact Hopkinson pressure bars., Rev. Sci. Instrum. 87 (2016) 23101. doi:10.1063/1.4940935.
[35] C.M. Sellars, W.J. McTegart, On the mechanism of hot deformation, Acta Metall. 14 (1966) 1136–1138. doi:10.1016/0001-6160(66)90207-0.
[36] A.K. Gupta, V.K. Anirudh, S.K. Singh, Constitutive models to predict flow stress in Austenitic Stainless Steel 316 at elevated temperatures, Mater. Des. 43 (2013) 410–418. doi:10.1016/j.matdes.2012.07.008.
[37] H.Y. Li, Y.H. Li, X.F. Wang, J.J. Liu, Y. Wu, A comparative study on modified Johnson Cook, modified Zerilli-Armstrong and Arrhenius-type constitutive models to predict the hot deformation behavior in 28CrMnMoV steel, Mater. Des. 49 (2013) 493–501. doi:10.1016/j.matdes.2012.12.083.
[38] X. Xiao, G.Q. Liu, B.F. Hu, X. Zheng, L.N. Wang, S.J. Chen, A. Ullah, A comparative study on Arrhenius-type constitutive equations and artificial neural network

model to predict high-temperature deformation behaviour in 12Cr3WV steel, Comput. Mater. Sci. 62 (2012) 227–234. doi:10.1016/j.commatsci.2012.05.053.
[39] D. TRIMBLE, G.E. O'DONNELL, Flow stress prediction for hot deformation processing of 2024Al-T3 alloy, Trans. Nonferrous Met. Soc. China. 26 (2016) 1232–1250. doi:10.1016/S1003-6326(16)64194-8.
[40] D. Trimble, G.E. O'Donnell, Constitutive Modelling for elevated temperature flow behaviour of AA7075, Mater. Des. 76 (2015) 150–168. doi:10.1016/j.matdes.2015.03.062.